

# UNSTEADY FLOW PHENOMENA IN INDUSTRIAL CENTRIFUGAL COMPRESSOR STAGE

L. Bonciani, L. Terrinoni, and A. Tesei  
Nuovo Pignone  
50127 Florence, Italy

## SUMMARY

It is well known that rotating non-uniform flow pattern has a strong influence on high pressure centrifugal compressor vibrations. This paper shows the results of an experimental investigation on a typical centrifugal compressor stage running on an atmospheric pressure test rig. Unsteady flow was invariably observed at low flow well before surge. In order to determine the influence of the statoric components, the same impeller was repeatedly tested with the same vaneless diffuser, but varying return channel geometry. Experimental results show the strong effect exerted by the return channel, both on onset and on the behavior of unsteady flow. Observed phenomena have been found to confirm well the observed dynamic behavior of full load tested machines when gas density is high enough to cause appreciable mechanical vibrations. Therefore, testing of single stages at atmospheric pressure may provide a fairly accurate prediction of this kind of aerodynamic excitation.

## INTRODUCTION

Problems which have arisen in past years with high density centrifugal compressors have considerably increased the demand for full load testing (ASME PTC 10, Class 1), mainly aimed at checking the stability of machines under aero-induced excitation forces.

Present experience leaves no doubts that aerodynamic excitation is always present in centrifugal compressors and it is obvious that the forces involved become more marked the greater gas density and machine speed. This is the reason why machines subject to aero-induced vibrations have been found more frequently in natural gas injection or urea synthesis plants than in ammonia synthesis or refinery compressors, even when running at the same pressure levels (ref. 1). Although the action of aerodynamic forces involved leads to subsynchronous vibrations in general, two completely different behaviors have been encountered: self-excited vibrations and forced vibrations. Vibrations belonging to the first category (self-excited vibrations) have been noted in high performance turbo-machinery (ref. 2) including high pressure compressors (ref. 3 and 4), apparently with greater frequency in back-to-back versions of the latter. The vibration frequency observed is normally the fundamental bending natural frequency of the rotor. An explanation commonly given for this phenomenon is based on destabilizing forces caused by the labyrinth seals (ref. 5 and 6). On the other hand vibrations belonging to the second category

(forced vibrations) have been recorded in all high density compressors. They have the following typical behavior (ref. 7 and 8):

- . They appear relatively near to surge and are very stable in amplitude.
- . Asynchronous frequency is very low (order of magnitude 10% of RPM)
- . Asynchronous amplitude depends on tip speed and gas density.

In order to examine this phenomenon more closely a test program was set up with the aim of investigating the amplitude and frequency of pressure oscillations within a centrifugal compressor stage. A standardized low specific speed stage, which is normally utilized in high pressure applications, was slated for testing.

#### SYMBOLS

R	Radius
p	static pressure
$P_o$	total pressure
$C_r$	radial velocity
A	pressure oscillations amplitude
$f_s$	fundamental frequency of pressure oscillations
$\Omega$	impeller angular velocity
$\hat{A}$	amplitude of pressure oscillations normalized to stage total inlet pressure
$\hat{f}_s$	fundamental frequency of pressure oscillations normalized to impeller speed ( $\hat{f}_s = 2\pi f_s / \Omega$ )
Mu	tip speed Mach number
$Re$	Reynolds number (based on diffuser axial width)
$\varphi$	inlet flow coefficient
$\hat{C}_r$	normalized radial velocity ( $\hat{C}_r = C_r / \Omega R$ )
$\alpha$	absolute flow angle (referred to tangential direction)
$C_p$	pressure recovery coefficient

Subscripts:

10	= measured at section 10
10	= " " " 10'
20	= " " " 20

20'	=	"	"	"	20'
30'	=	"	"	"	30'
40	=	"	"	"	40
40'	=	"	"	"	40'
50'	=	"	"	"	50'
60	=	"	"	"	60
60'	=	"	"	"	60'
D	=	diffuser			
RC	=	return channel			
*	=	onset of unsteady flow			

#### TEST FACILITIES AND INSTRUMENTATION

Tests have been arranged on one of the three test rigs available for the individual stages development (ref. 9). A cross section of the test rig is shown on Fig. 1; the stage consisted of an impeller, a free vortex diffuser, a cross-over and a return channel. The gas utilized was air at atmospheric pressure in an open loop circuit. Speed was adjusted by an hydraulic coupling torque converter while an electrically actuated discharge valve was operated to vary the pressure ratio. Table 1 shows the conventional instrumentation used for industrial stage testing. Table 2 shows the instrumentation utilized to detect pressure oscillations connected with non-stationary flow conditions. The following should be mentioned of the conventional instrumentation:

- . The data acquisition system is based on a Solartron system 35 with a PDP 11/03 control unit.
- . All pressure readings are connected, through a scannivalve, to a single pressure transducer. The transfer function of the measurement chain has been experimentally tested, to check that the output is the time average of the pressure within the frequency range of interest.

Regarding non-stationary reading we can note that:

- . static pressure probes are the Kulite XT-190-50 type
- . total pressure probes are the Kulite XB-093-50G type
- . probe signals have been recorded on an Ampex PR 2200 tape recorder and finally analyzed through an Ono-Sokki CF-500 real time spectrum analyzer. Data shown for each tested point are the RMS averages of 256 spectra.

Two different stage configurations have been tested: configuration A and configuration B. Both configurations utilize the same impeller and diffuser but different return channels and, of course, cross-overs.

## TEST RESULTS

### Configuration A

It is necessary to point out that the following procedure was adopted to obtain the data relating to configuration A.

1. Readings were taken of time "average" quantities (i.e. pressures, temperatures etc. at the different measuring sections) with conventional instrumentation.
2. Next, readings were taken of pressure oscillations (remeasuring inlet pressure, flow and RPM) independently of prior readings.
3. Finally some "points" were repeated in regions of particular interest.

### Qualitative Description

When flow is reduced at constant speed the following behavior was observed:

- . Pressure oscillations started simultaneously on all pressure transducers with very low amplitude and almost sinusoidal shape.
- . A small flow reduction resulted in a slight increase in frequency and a considerable increase in amplitude while the signal shape remained sinusoidal.
- . If flow was further reduced the phenomena observed was dependent on the tip speed Mach numbers ( $\mu$ ) as follows:

At  $\mu = 0.45$  and  $0.60$  we noted:

- . The shape of the signal suddenly changed from a sinusoid with a frequency of  $f_s$  to a signal having frequencies  $f_s$  and  $f_s/2$  with comparable amplitudes. The onset of the second frequency (i.e.  $f_s/2$ ) is usually very sudden.
- . When flow was reduced the  $f_s$  and  $f_s/2$  frequencies slowly increased and the  $f_s$  amplitude component remained almost constant while the  $f_s/2$  one rose gradually.
- . On rethrottling, the  $f_s/2$  signal finally disappeared and the  $f_s$  signal had a sudden increase in amplitude.
- . Further flow reductions caused a shifting of the  $f_s$  frequency while amplitude remained almost constant till full surge.
- . On opening the valve and exploring the phenomenon starting from full surge we found that frequencies and amplitudes were repetitive related to flow. A slight hysteresis was noted in the onset region.

At  $\mu = 0.75$  and  $0.85$  we observed that:

- . Pressure oscillations might have a sinusoidal shape with  $f_s$  frequency till full surge.

- . With the same inlet flow coefficient it was possible to shift from a single frequency signal ( $f_s$ ) to a dual-frequency signal having the same  $f_s$  frequency and an additional component at  $f_s/2$  frequency. Each one of the amplitudes (i.e. at  $f_s$  and  $f_s/2$ ) with dual frequency was lower than the amplitude with single frequency.

Although the factors governing the shift from one shape to the other were not discovered, the following observations were made:

- a. The shift from a single frequency shape to the other seemed easier when increasing the flow from the surge.
- b. Sometimes introduction of the conventional instrumentation probes into the diffuser was very effective in triggering the shift to the dual-frequency shape.
- c. Maintaining a constant opening of the discharge valve and raising the speed from low  $Mu$  (i.e.  $Mu = 0.45$ ) with dual frequency shape the signal might retain the same shape even if  $Mu$  exceeds 0.85.
- d. Cases were observed where shifting appeared several minutes after the last positioning of the valve.

Summarizing we believe that the phenomenon can be described as follows:

- . The unsteady flow pattern may exhibit two distinct shapes (single frequency and dual frequency).
- . The dual frequency shape is stable within a range of flows-RPM (or better  $\varphi - Mu$ ) and metastable in the remaining range.
- . When dual frequency exists it may survive in the entire speed range explored.

It will later be seen that the two different signal shape correspond to two distinct values of the return channel recovery coefficient, based on time average.

#### Quantitative Description

To keep the length of the paper within reasonable limits we will indicate only the results obtained at section 20', behavior at all the other measuring sections being very similar.

Fig. 2 shows the frequencies normalized to the RPM while fig. 3 and 4 show the amplitudes of the pressure oscillations corresponding to  $f_s$  and  $f_s/2$  normalized to the suction pressure. The following can be remarked:

- . Amplitudes at section 10' (impeller suction) were always negligible till surging.
- . At the different measuring sections pressure oscillations amplitudes exhibited shapes similar to those shown for section 20'. The following are the average values found:

at  $f_s$  (with both single and dual  
frequency shape)

---

$$\begin{aligned} A_{30'} &\approx 80\% A_{20'} \\ A_{40'} &\approx 60\% A_{20'} \\ A_{50'} &\approx 60\% A_{20'} \\ A_{60'} &\approx 9\% A_{20'} \end{aligned}$$

at  $f_s/2$

---

$$\begin{aligned} A_{30'} &\approx 81\% A_{20'} \\ A_{40'} &\approx 60\% A_{20'} \\ A_{50'} &\approx 17\% A_{20'} \\ A_{60'} &\approx 9\% A_{20'} \end{aligned}$$

- . Irrespectively of the flow coefficient, the phase difference between static probes at the same radius is  $90^\circ$  for the  $f_s/2$  component and  $180^\circ$  for the  $f_s$  component with dual frequency signal shape and is  $180^\circ$  for the  $f_s$  component when the signal is single-frequency. Therefore it seems that  $f_s/2$  is associated with a single stall cell, while  $f_s$  is associated with two stall cells.
- . The phase difference between static probes at the same angular position was practically independent from the flow coefficient. Typical values measured (in round figures) were:  $-10^\circ$ , between sec. 20' and sec. 30', and  $-20^\circ$ , between sec. 20' and sec. 40', for the  $f_s$  component (with both single or dual frequency shape) and always near  $0^\circ$  for the  $f_s/2$  component.

#### Analysis of Time Averaged Data

Fig. 5, 6 and 7 show the pressure ratios (static to total and total to total) versus flow at three different measuring sections. An appreciable variation in the slope can be noted at the onset of the pressure oscillations followed by a region with a positive slope. At  $Mu = 0.75$  and  $0.85$  two distinct branches clearly identify the working regions relevant to the two shapes of the signal previously described.

The lack of connection between "average" measurements and instantaneous measurements initially led to considerable confusion. Only later was it realized that the two disturbance shapes have distinct "average" measurements and that the shift from one shape to the other cannot always be triggered at will in the  $Mu = 0.75+0.85$  area. As a result the graphs in fig. 7 and fig. 3 are slightly contradictory: the shift point from one shape to the other at  $Mu = 0.75$  and  $Mu = 0.85$ , shown in fig. 3, does not coincide with those indicated in fig. 7. The general shape of the amplitude curve at  $Mu = 0.75$  looks similar to those at  $Mu = 0.45$  and  $Mu = 0.60$  but fig. 7 suggests that this was not always the case.

The flow coefficients corresponding to the onset of the pressure oscillations are related to tip speed Mach numbers. However, if the inlet flow coefficient is plotted versus any of the impeller exit variables, for example  $\hat{C}_{r20}$ , as shown

on fig. 8, one can note that the onset starts at an almost constant value of such variables. Fig. 9 shows both  $\alpha_{20}$  and  $\alpha_{40}$  versus  $\hat{C}_{r20}$ . It can be noted that the unsteady flow condition invariably appears when  $\alpha_{20*} \simeq 10^\circ$  and  $\alpha_{40*} \simeq 13^\circ$ . The behavior of the diffuser pressure recovery coefficient, see fig. 10, shows considerable scattering corresponding to the  $\alpha_{20*}$  onset value. Fig. 11 shows that the return channel pressure recovery coefficient exhibits considerable discontinuity in the onset regions. It is of particular interest to note that the  $C_{pRC}$  vs.  $\alpha_{40}$  curve is split into two different branches which correspond to dual frequency and single frequency respectively.

Bearing in mind, that pressure oscillations at impeller suction were always negligible and considering the behavior of pressure recovery coefficients, it seems that the phenomenon had its origin from the statoric components. Three different hypothesis can be formulated to explain the onset mechanism:

- a. - the phenomenon pertains to the diffuser "in itself" and starts when a "critical" inlet angle is reached.
- b. - the phenomenon pertains to the return channel "in itself" and starts when a "critical" incidence angle is reached.
- c. - interaction between the vaneless diffuser and return channel is not negligible, therefore a "critical value" of some exit variable exists which cannot be clearly ascribed to each one individually.

It is clear that these hypothesis as they have been formulated are somewhat simplified and that they ignore the fact that the inlet conditions of the stationary components, for a constant value of  $\hat{C}_{r20}$ , are not strictly similar at different  $\mu$ . For instance:

- "average" velocity profiles are not exactly similar
- the diffuser inlet absolute Mach number increases from 0.25 at  $\mu = 0.45$  to 0.43 at  $\mu = 0.85$
- the diffuser inlet Reynolds number varies from  $Re = 90,000$  at  $\mu = 0.45$  to  $Re = 160,000$  at  $\mu = 0.85$

However these variations are moderate and fig. 9, fig. 10 and fig. 11 suggest that the influence of these factors is limited within the range explored throughout testing.

Let us assume as a working hypothesis that the phenomenon is mainly influenced by the return channel and starts when a "critical" incidence angle at the leading edge of the return channel blades is reached. In the light of this hypothesis a new return channel was built with identically shaped blades, but a different axial width, to move the onset close to the design flow of the stage.

## Configuration B

In order to avoid some confusion experienced when testing configuration A, both time averages and instantaneous measurements were acquired contemporaneously, moreover the tested points were concentrated in the unsteady flow area.

The phenomenon is easier to describe since it is characterized by a single-frequency shape within the tested range of  $\mu$ . The onset as well as the growth of the pressure oscillations are similar to those tested on configuration A when the single frequency shape was present. Fig. 12 and fig. 13 show respectively the normalized frequency and the pressure oscillations amplitudes at sec. 20' versus the inlet flow coefficient. The following can be noted:

- . Amplitudes at sect. 10' are always negligible till full surge.
- . At the different measuring sections pressure oscillations amplitudes are qualitatively similar to those of section 20'. The following are the average values found:

$$\begin{aligned}A_{30'} &\approx 78\% A_{20'} \\A_{40'} &\approx 60\% A_{20'} \\A_{50'} &\approx 56\% A_{20'} \\A_{60'} &\approx 14\% A_{20'}\end{aligned}$$

Irrespective of the flow coefficient, the phase difference between static probes at the same radius is  $180^\circ$  thus indicating a two stall cells configuration.

- . The phase difference between static probes at the same angular position was slightly dependent on the flow coefficient. Starting from the onset and reaching the full surge, the phase difference gradually changed (in round figures) from  $0^\circ$  to  $-10^\circ$ , between sec. 20', and 30', and from  $0^\circ$  to  $-20^\circ$  between sec. 20' and 40', being the phase difference ratio almost constant and near to two. As a consequence, loci of maximum and minimum pressure amplitudes are not radial lines but curves shifted slightly backwards as referred to the direction of rotation.

### Analysis of the Time Averaged Data

Fig. 14, 15 and 16 show the pressure ratios (static to total and total to total) versus flow at three different measuring sections. It can be noted that the onset has been shifted to a considerably higher flow as indicated by the hypothesis formulated. As already noted with configuration A, the onset of pressure oscillations starts at an almost constant value of the impeller discharge parameters (see fig. 17 and fig. 18). In this case we had  $\alpha_{40*} \approx 18^\circ$  and  $\alpha_{20*} \approx 14^\circ$ .

It can be verified that the onset takes place when there is a practically constant incidence angle at return channel blades while flow angles along the diffuser are considerably different from those of the configuration A. Fig. 20 shows that the pressure recovery coefficient of the return channel again exhibits a sudden drop at the onset of unsteady flows. The  $C_{pD}$  too curves downwards, fig. 19, however the drop is less evident, whereas scattering is greatly reduced if compared with configuration A.

#### TESTS SUMMARY AND CONCLUDING REMARKS

Two different stage configurations were tested to study the behavior of unsteady flows. Configuration A and configuration B had identical impellers and diffusers but different return channels and cross-overs. The following can be concluded on the basis of tests performed:

1. The two configurations tested clearly showed that unsteady flow is caused by the statoric components.
2. With configuration B unsteady flows begin at much higher flow coefficient than those of configuration A.
3. The onset of pressure oscillations takes place with considerably different diffuser flow angles for the two configurations, while the incidence angle at the return channel blades is almost constant.

Therefore it seems that the return channel blades played the most important role in determining both the onset and the growth of the phenomenon.

To conclude, some additional remarks are necessary to give an indication of the general validity of obtained results and some comparison with the behavior of complete machines when gas density is high enough to reveal pressure oscillations in the form of shaft vibrations.

- . Tests performed on completely different stages (i.e. several standard stages for average specific speed and one 3-D type typical for pipeline applications) exhibited unsteady flows with frequency-amplitude behavior similar to that of the configurations described in this paper.
- . The frequencies of forced asynchronous vibrations, detected in full load testing of high density compressors (ref. 7 and 8) showed a very good correspondence to the frequencies of pressure oscillations of non stationary flows investigated on a single stage test rig.
- . Reviewing current literature on this subject the following can be remarked:
  - a. The tests referred to with ref. 10, 11, 12 and 13 definitely show that a vaneless radial diffuser may generate self-excited pressure oscillations. The present paper suggests that such data should be used with some caution for an industrial centrifugal stage, having a return channel.

- b. Test results of the present paper agree to a great extent with ref. 14 and with some of the data published in ref. 15, both based on testing of industrial centrifugal stages with return channels.

#### REFERENCES

1. Ferrara P.L., Tesei A.: High Pressure Centrifugal Compressors. Inst. Mech. Eng. Conference Publications 1978-3 March 1978
2. EK M.C.: Solution of the Subsynchronous Whirl Problem in the High Pressure Hydrogen Turbomachinery of the Space Shuttle Main Engine. AIAA/SAE 14-th Joint Propulsion Conference. Las Vegas, Nev.-July 25-27, 1978.
3. Geary C.H., Damratowsky L.P., Seyer C.: Design and Operation of the World's Highest Pressure Gas Injection Centrifugal Compressor paper No. O.T.C. 2485 presented at the Offshore Technology Conference, Houston Texas, May 1976.
4. Coletti N.J., Crane M.E.: Centrifugal Compression on the Arun High Pressure Injection Project. Inst. mech. Eng. Conference Publications 1981-3 March 1981.
5. Wright D.V.: Air Model Tests of Labyrinth Seal Forces on a Whirling Rotor. ASME Book Editor W.G. Steltz 1977.
6. Benckert H., Wachter J.: Flow Induced Spring Coefficients of Labyrinth Seals for Application in Rotor Dynamics. NASA Conference Publication 2133-Aug. 1980.
7. Bonciani L., Ferrara P.L., Timori A.: Aero-Induced Vibration in Centrifugal Compressors. NASA Conference Publication 2133-August 1980.
8. Sabella D., Terrinoni L., Timori A.: Full Load Testing of Centrifugal Natural Gas Injection Compressors. Inst. Mech. Eng. Conference Publication 1981-3 March 1981.
9. Benvenuti E.: Aerodynamic Development of Stages for Industrial Centrifugal Compressors, Part. 1 & 2 - ASME Paper No. 78-GT4 & 5.
10. Jansen W.: Rotating Stall in a Radial Vaneless Diffuser. Transactions of the ASME--Journal of Basic Engineering - Dec. 1964 p.p. 750+758.
11. Abdelhamid A.N., Bertrand J.: Distinctions Between Two Types of Self-excited Gas Oscillations in Vaneless Radial Diffusers - ASME Paper No. 79-GT-58.
12. Abdelhamid A.N.: Analysis of Rotating Stall in Vaneless Diffusers of Centrifugal Compressors. ASME Paper No. 80-GT-184.
13. Abdelhamid A.N.: Effects of Vaneless Diffuser Geometry on Flow Instability in Centrifugal Compression Systems. ASME Paper No. 81-GT-10.
14. Abdelhamid A.N., Colwill W.H., Barrows J.F.: Experimental Investigation of Unsteady Flow Phenomena in Vaneless Radial Diffusers. ASME Paper No. 78-GT-23.
15. Van Den Braembussche R.A., Frigne P., Roustan M.: Rotating non Uniform Flow in Radial Compressors. AGARD C.P. 282-May 1980

TABLE 1.

Measuring sect.	Total pressure probes	Static pressure probes	Thermoel.
Sec. 10 (impeller inlet)	4 Kiel 1 cobra	1	8 (circum. and radially spaced)
Sec. 20 (diffuser inlet)	1 cobra	1	2
Sec. 40 (diffuser exit)	1 cobra	4	
Sec. 60 (return channel exit)	4 Kiel	8 (4+4 at inner and over radius)	8 (circum. and radially spaced)

TABLE 2.

Measuring sect.	Total pressure probes	Static pressure probes
Sec. 10' (Impeller inlet)	1	1
Sec. 20' (Diffuser inlet)	1	2 (90° spaced)
Sec. 30' (Diffuser midspan)	1	2 (90° spaced)
Sec. 40' (Diffuser exit)		2 (90° spaced)
Sec. 50' (Return channel throat area)		2 (90° spaced. Throat area of two sections of the return channel)
Sec. 60' (Return channel exit)		1 (At the exit of one of the two sections of sec. 50')

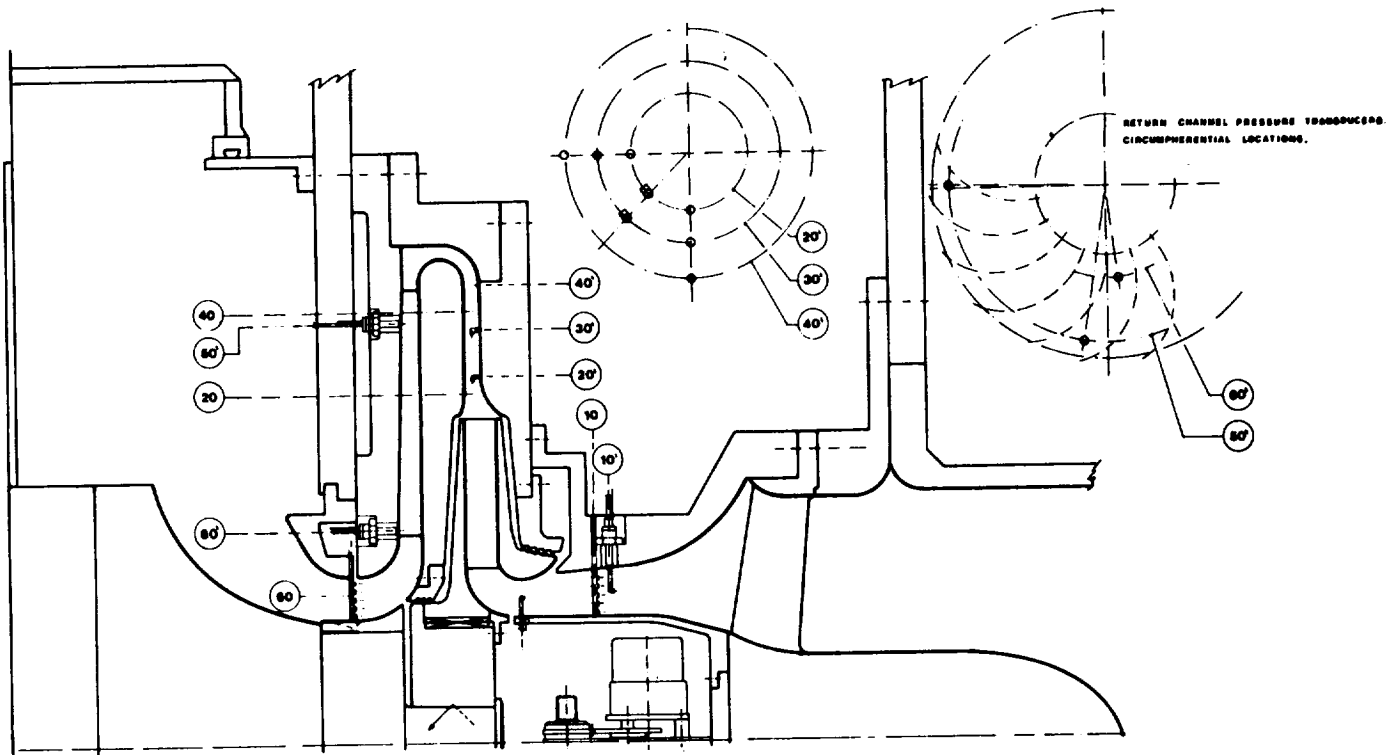


Figure 1. - Cross section of the test rig.

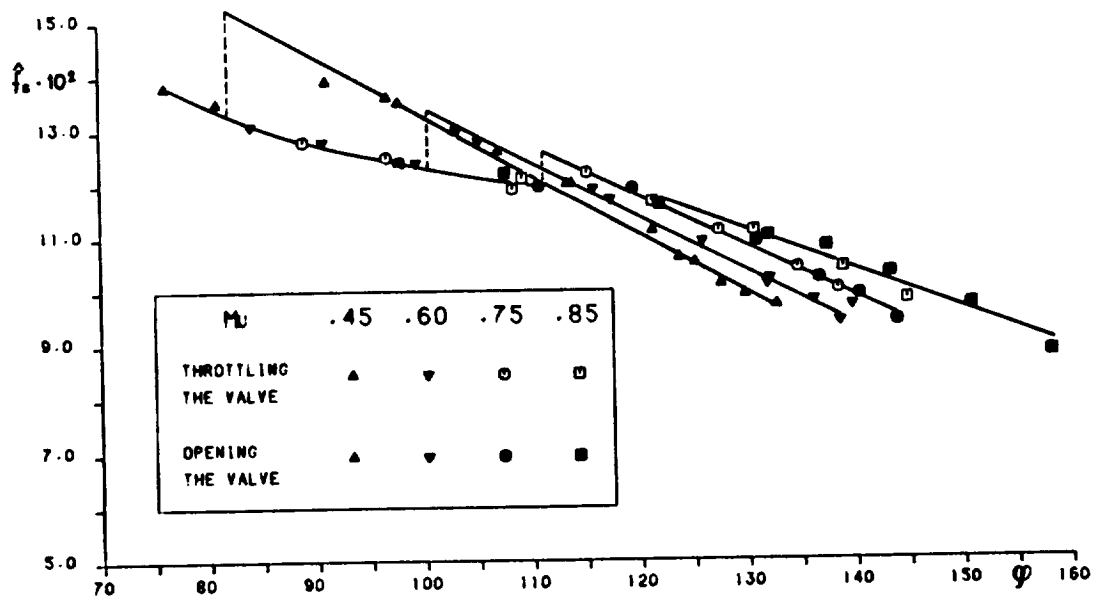


Figure 2. - Normalized observed frequency vs. inlet flow coefficient (configuration A).

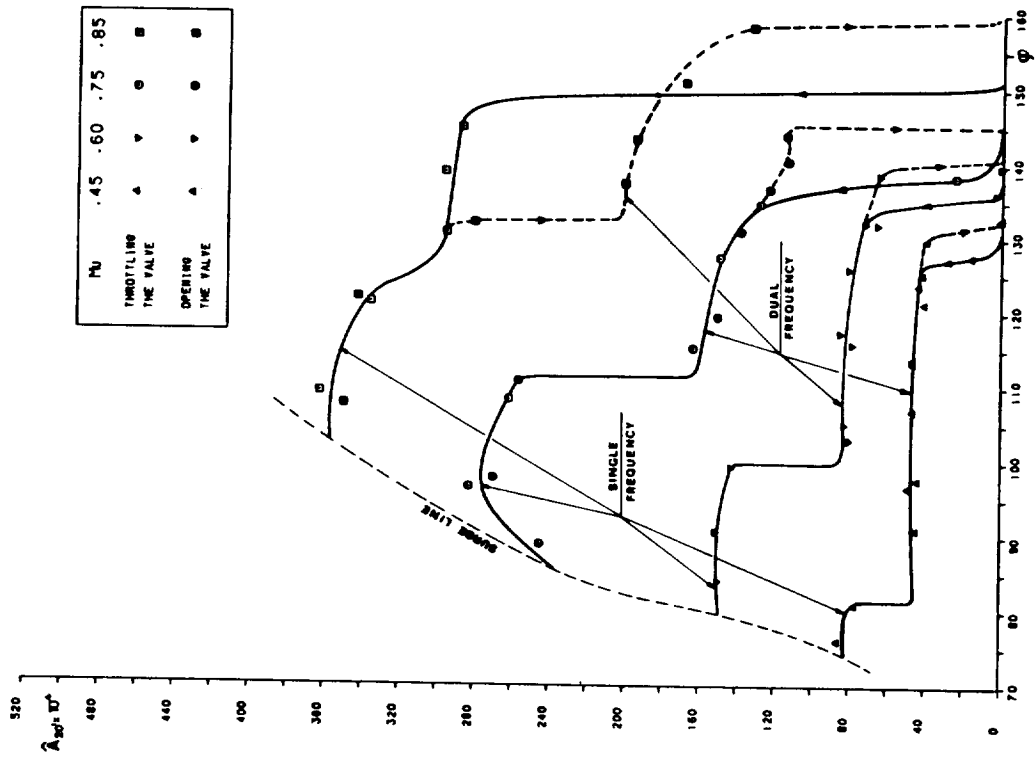


Figure 3. - Static pressure oscillation reduced amplitude ( $\hat{p}$  fs) at section 20 vs. inlet flow coefficient (configuration A).

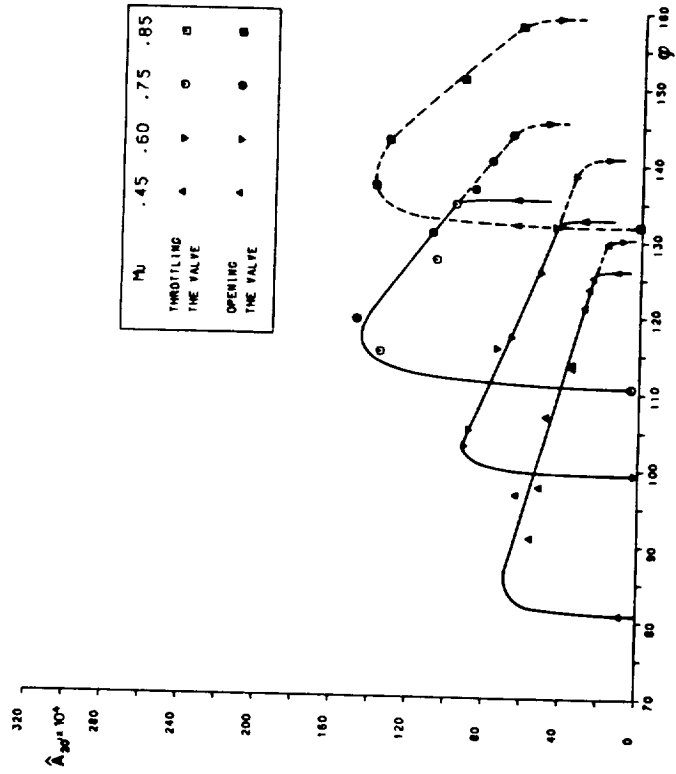


Figure 4. - Static pressure oscillation reduced amplitude ( $\hat{p}$  fs/2) at section 20 vs. inlet flow coefficient (configuration A).

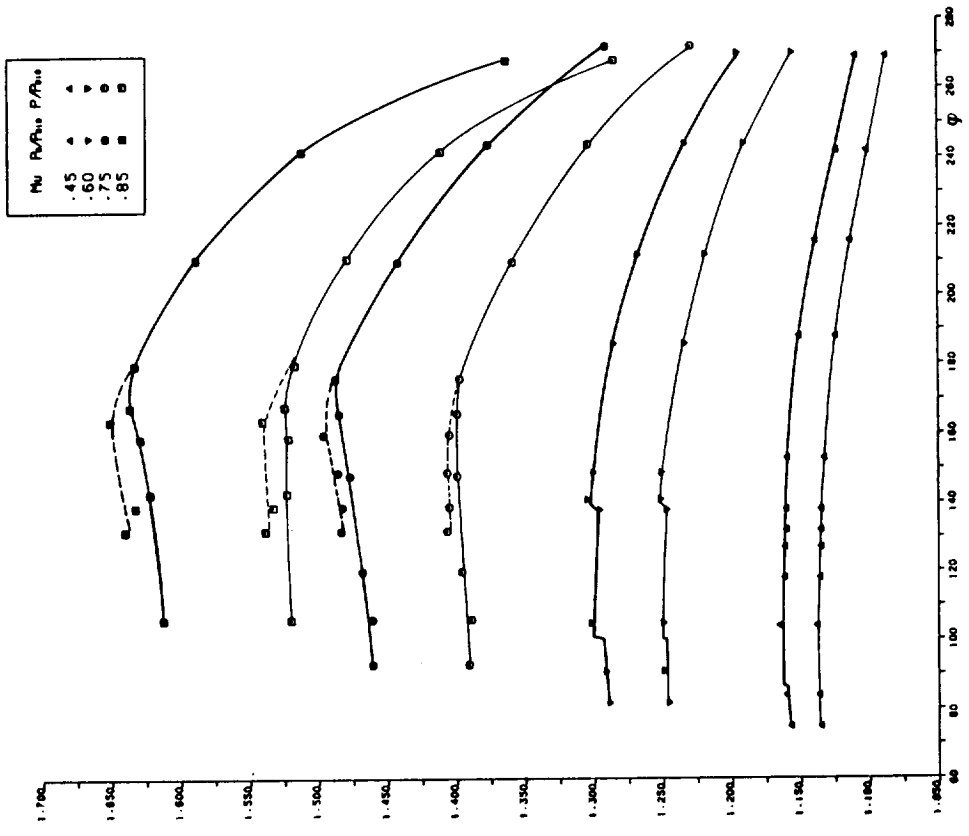


Figure 5. - Static to total and total to total pressure ratios at section 20 vs. inlet flow coefficient at different Mach numbers (configuration A).

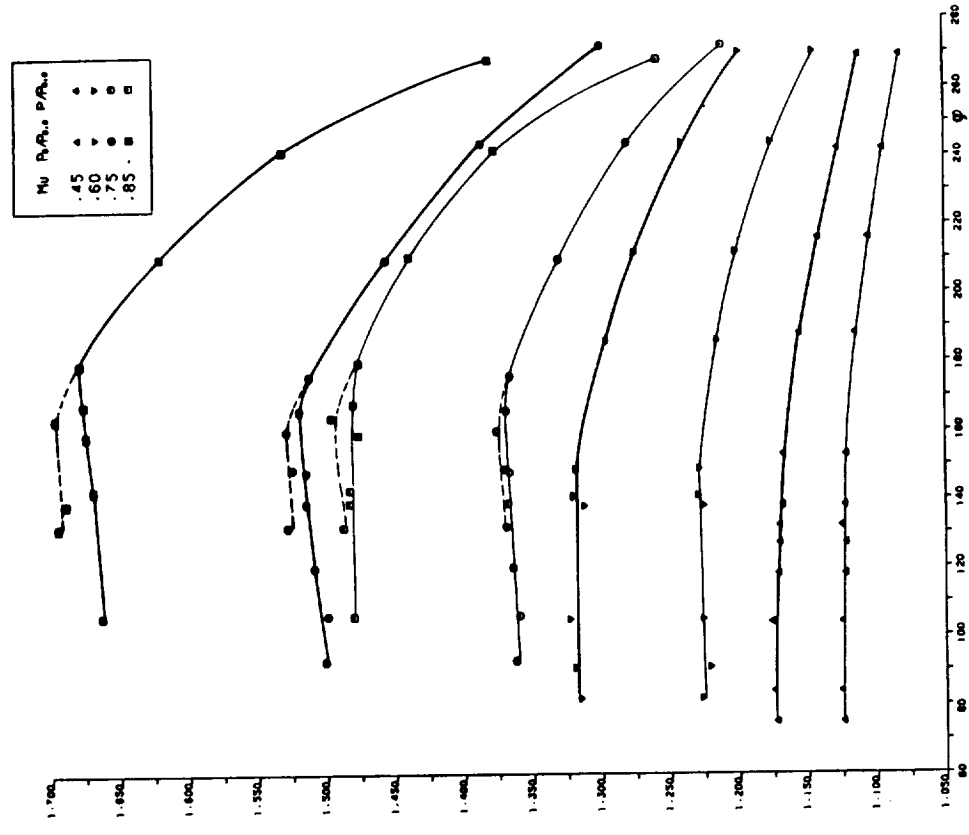


Figure 6. - Static to total and total to total pressure ratios at section 40 vs. inlet flow coefficient at different Mach numbers (configuration A).

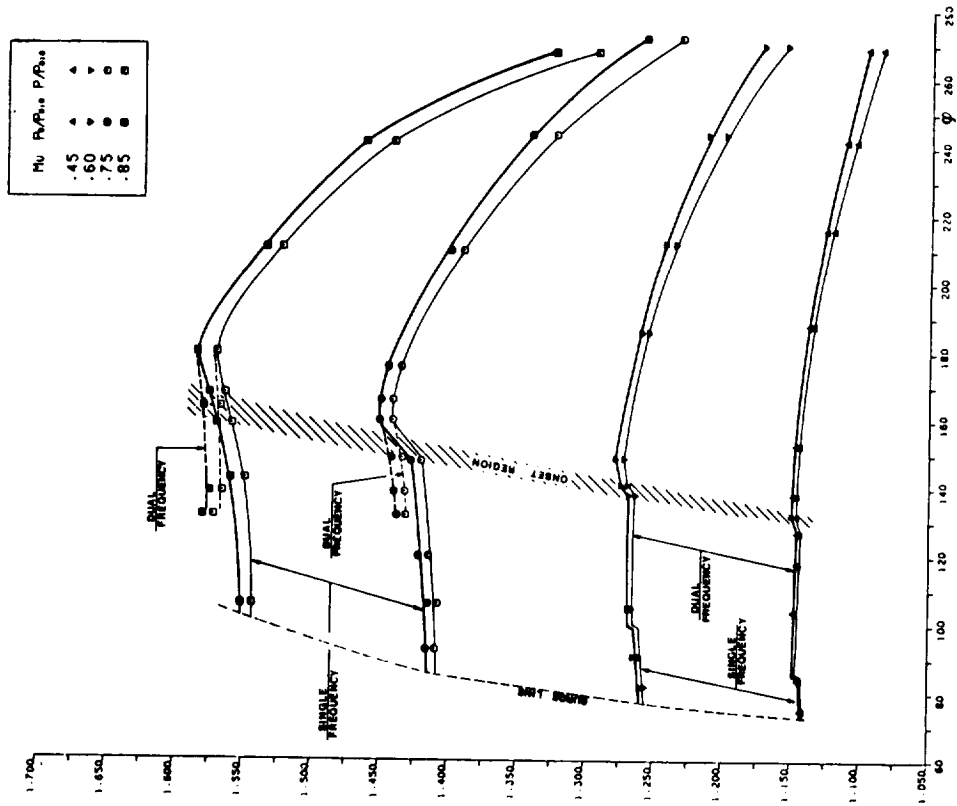


Figure 7. - Static to total and total to total pressure ratios at section 60 vs. inlet flow coefficients at different Mach numbers (configuration A).

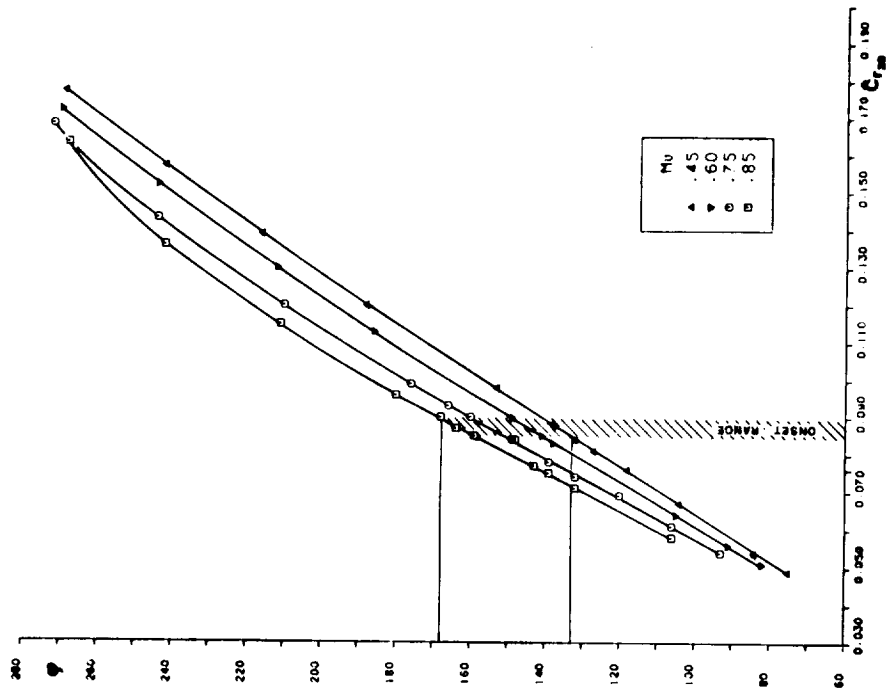


Figure 8. - Flow coefficient versus nondimensional radial speed at section 20, at different Mach numbers (configuration A).

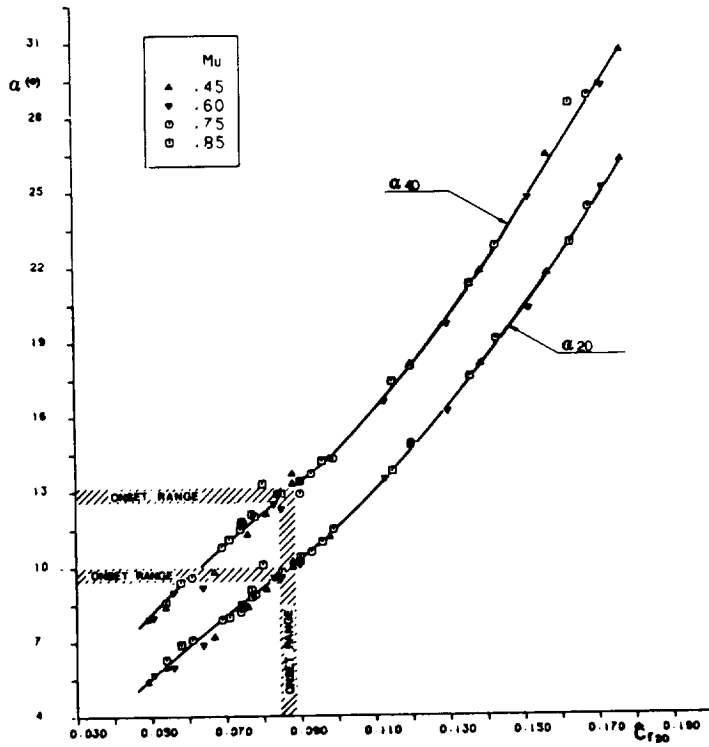


Figure 9. - Absolute flow angles at section 20 and section 40 vs. nondimensional radial speed at section 20 (configuration A).

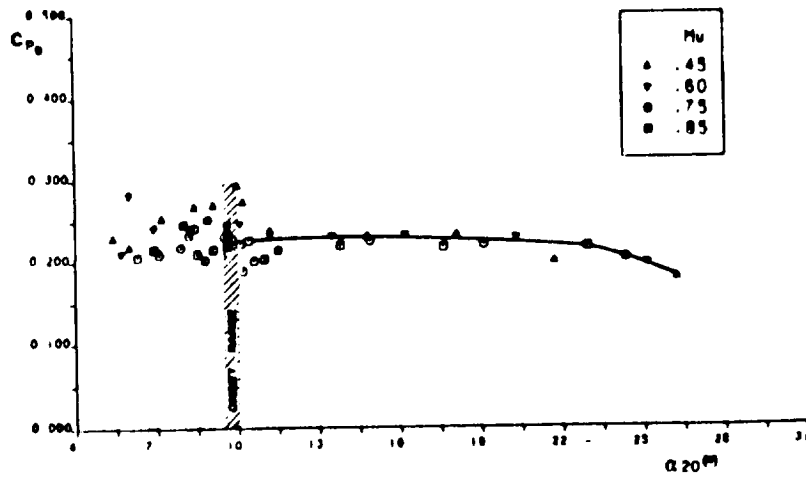


Figure 10. - Vaneless diffuser pressure recovery coefficient vs. absolute flow angle at section 20 (configuration A).

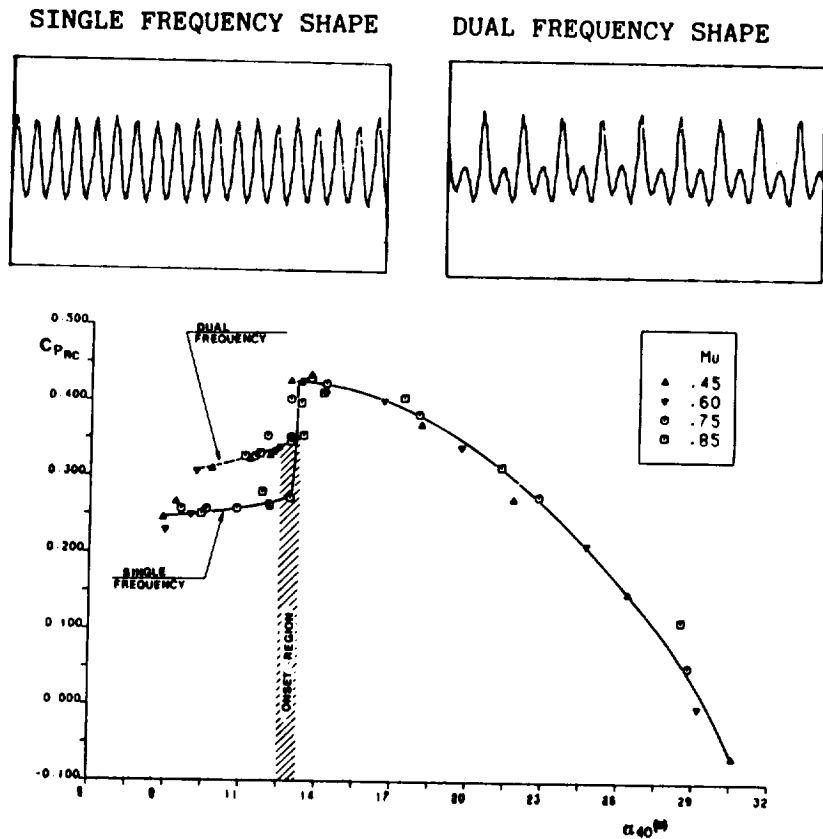


Figure 11. - Return channel pressure recovery coefficient vs. absolute flow angle at section 40 (configuration A).

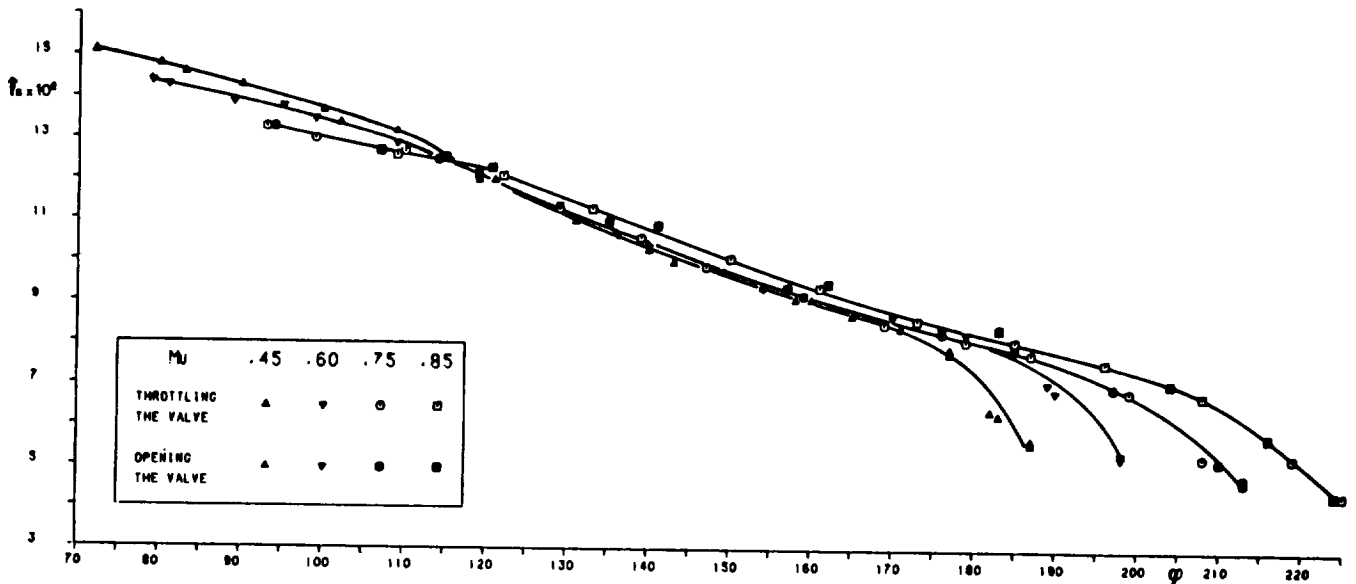


Figure 12. - Normalized observed frequency vs. inlet flow coefficient (configuration B).

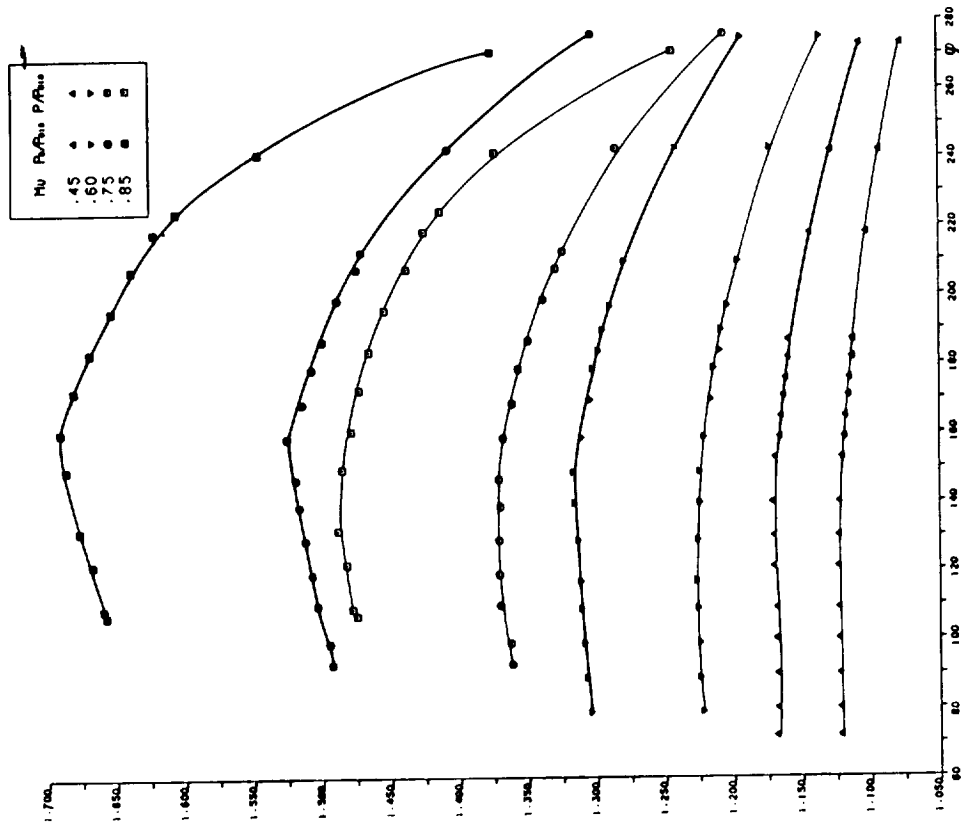


Figure 14. - Static to total and total to total pressure ratios at section 20 vs. inlet flow coefficient at different Mach numbers (configuration B).

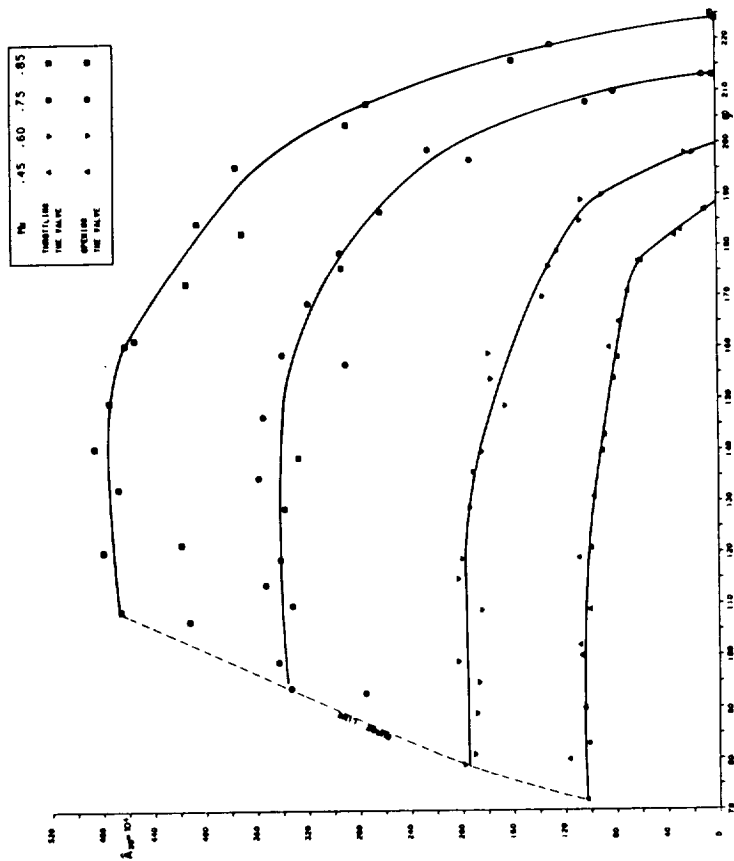


Figure 13. - Static pressure oscillation reduced amplitude ( $\theta$  fs) at section 20 vs. inlet flow coefficient (configuration B).

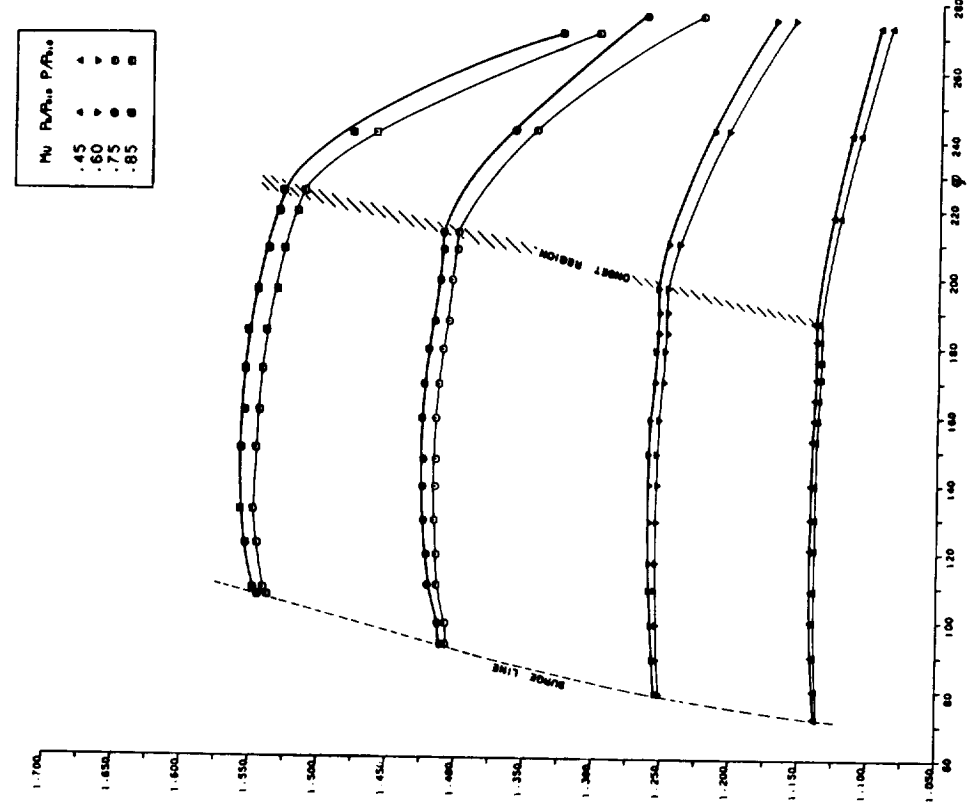


Figure 16. - Static to total and total to total pressure ratios at section 60 vs. inlet flow coefficient at different mach numbers (configuration B).

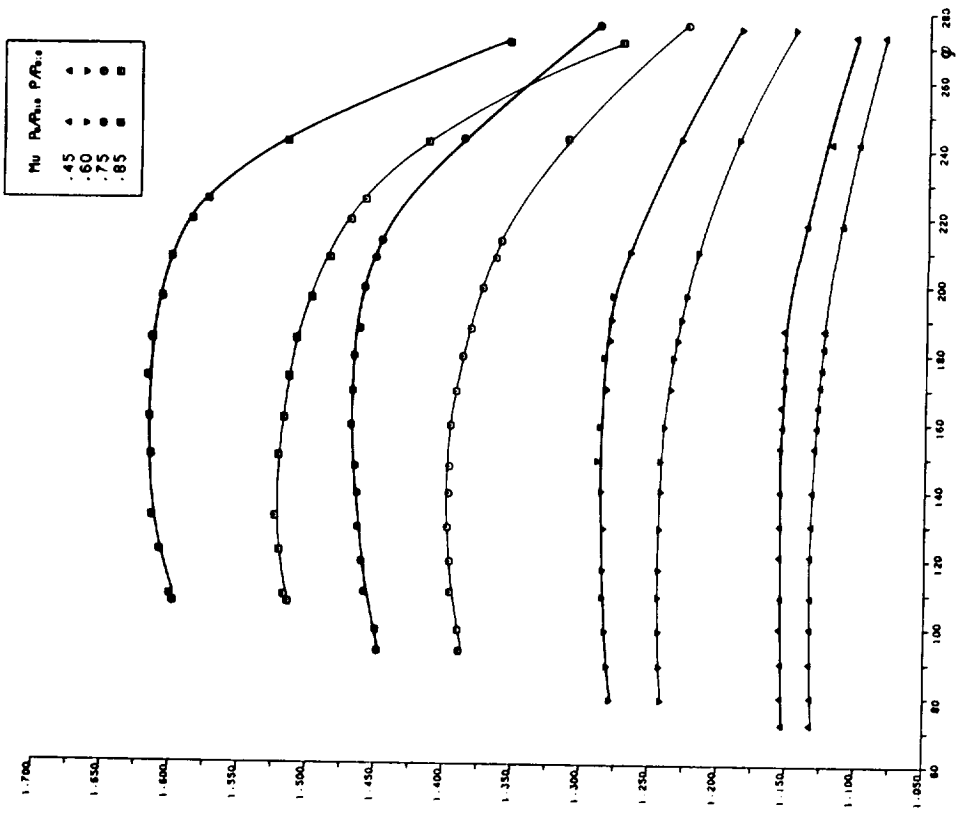


Figure 15. - Static to total and total to total pressure ratios at section 40 vs. inlet flow coefficient at different Mach numbers (configuration B).

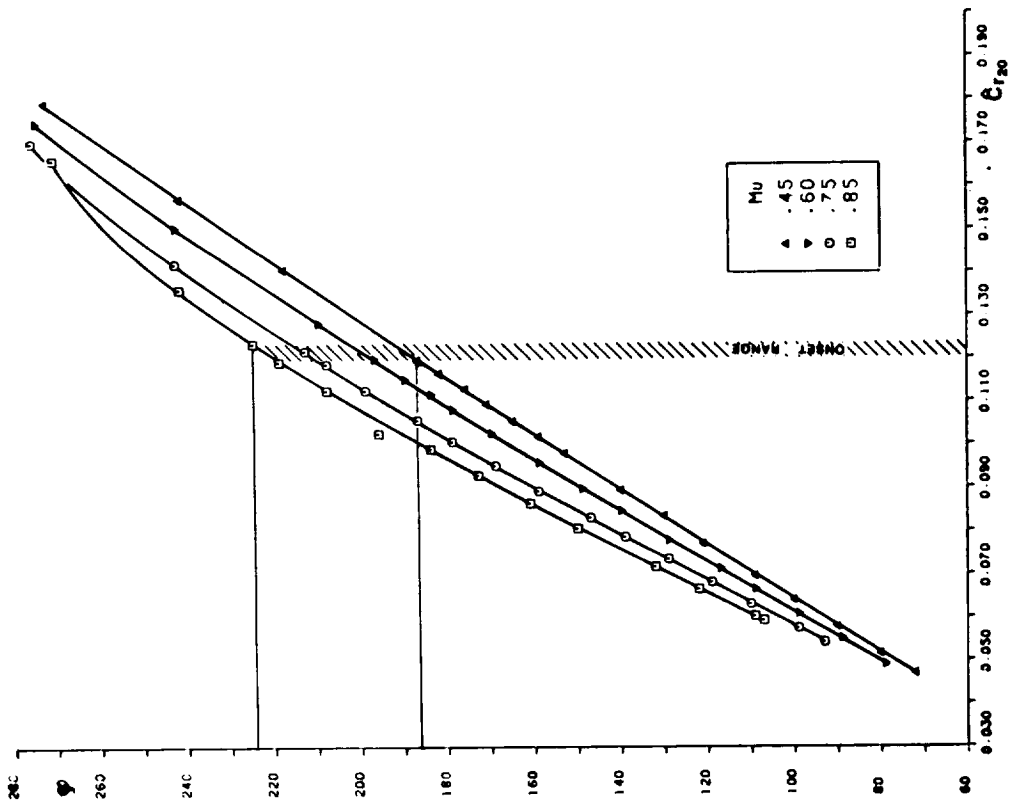


Figure 17. - Flow coefficient versus nondimensional speed at section 20, at different Mach numbers (configuration B).

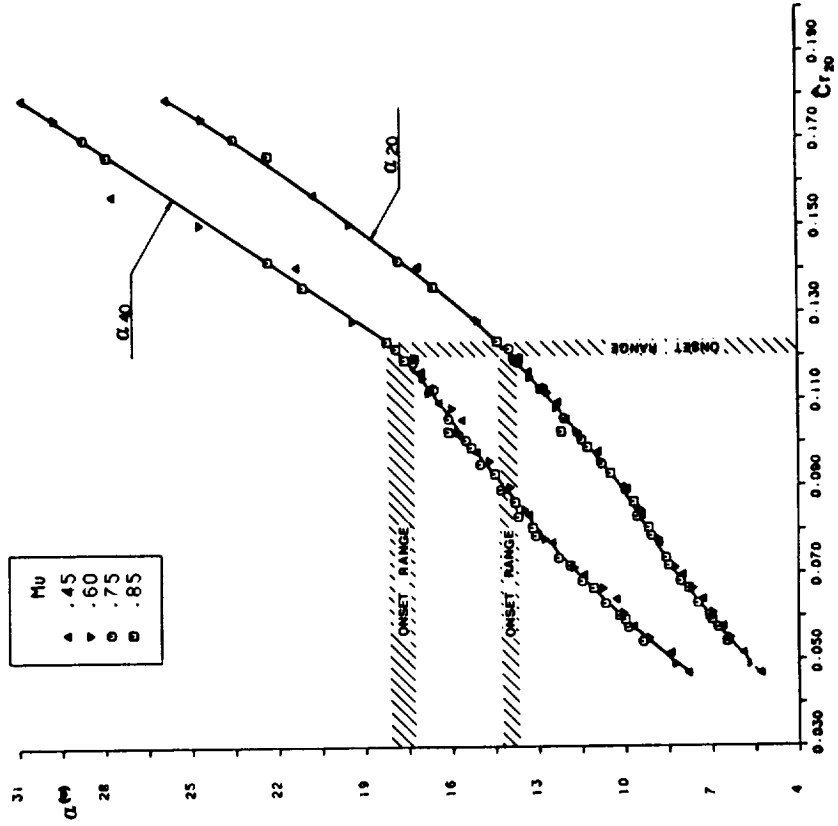


Figure 18. - Absolute flow angles at section 20 and section 40 vs. nondimensional radial speed at section 20 (configuration B).

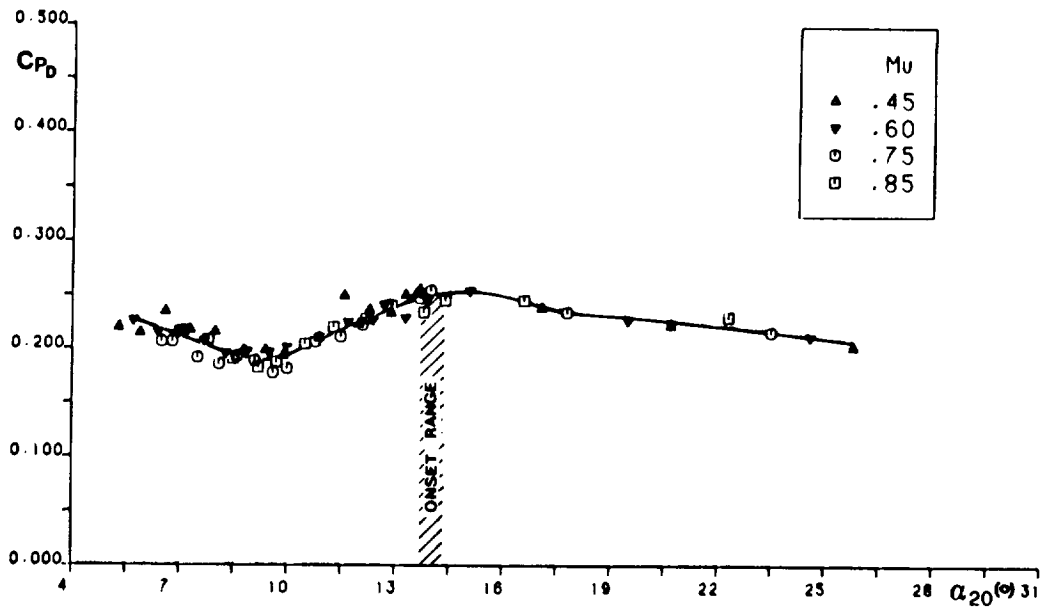


Figure 19. - Vaneless diffuser pressure recovery coefficient vs. absolute flow angle at section 20 (configuration B).

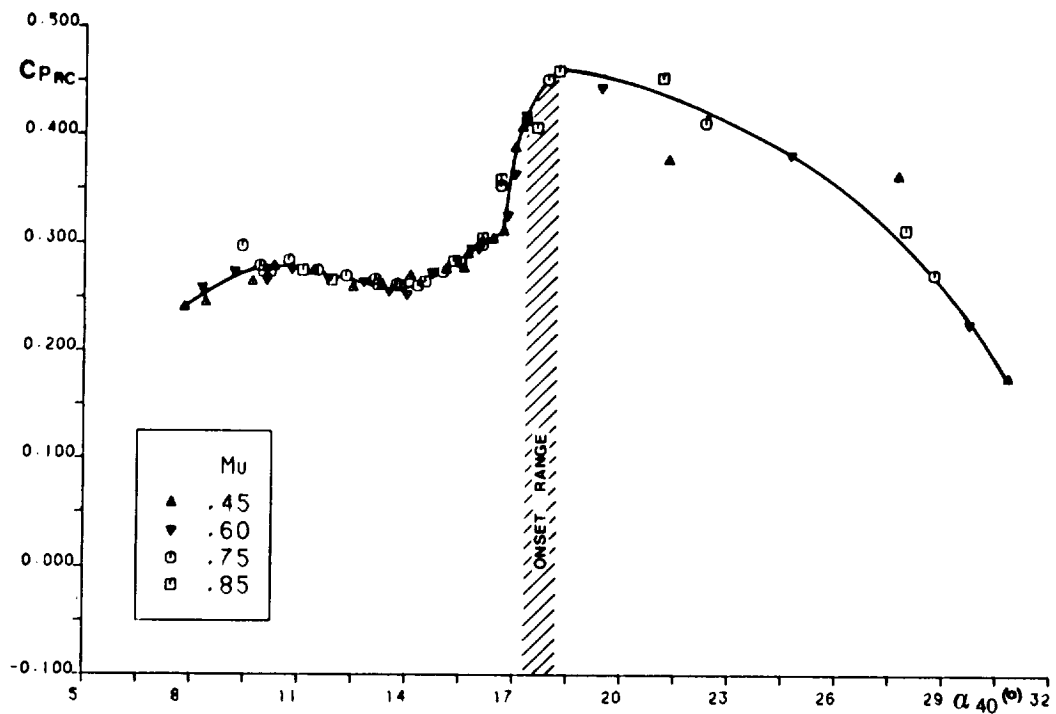


Figure 20. - Return channel pressure recovery coefficient vs. absolute flow angle at section 40 (configuration B).